SCIENCE CHINA
Information Sciences

• RESEARCH PAPER •

February 2025, Vol. 68, Iss. 2, 122401:1–122401:8
https://doi.org/10.1007/s11432-023-4070-8

Bulk photovoltaic effect in two-dimensional ferroelectric α-In_2Se_3

Huiting WANG[1,2], Shuaiqin WU[1,3*], Yan CHEN[1,3*], Qianru ZHAO[1,2], Jinhua ZENG[1,2], Ruotong YIN[1,2], Yuqing ZHENG[1,2], Chang LIU[1], Shukui ZHANG[1,5], Tie LIN[1], Hong SHEN[1], Xiangjian MENG[1*], Jun GE[1], Xudong WANG[1*], Junhao CHU[1,2,3] & Jianlu WANG[1,3,4]

[1]*State Key Laboratory of Infrared Physics, Shanghai Institute of Technical Physics, Chinese Academy of Sciences, Shanghai 200083, China*
[2]*University of Chinese Academy of Sciences, Beijing 100049, China*
[3]*Shanghai Frontiers Science Research Base of Intelligent Optoelectronics and Perception, Institute of Optoelectronics, Fudan University, Shanghai 200433, China*
[4]*Frontier Institute of Chip and System, Fudan University, Shanghai 200433, China*
[5]*Hangzhou Institute for Advanced Study, University of Chinese Academy of Sciences, Hangzhou 310024, China*

Received 8 December 2023/Revised 29 February 2024/Accepted 7 June 2024/Published online 17 December 2024

Abstract Non-centrosymmetric material systems can generate spontaneous photocurrent without a p-n junction under uniform illumination, which is known as the bulk photovoltaic effect (BPVE). It has garnered significant attention for its application potential in the fields of energy harvesting and photoelectric detection. In this study, we report the BPVE observed in two-dimensional ferroelectric α-In_2Se_3 multilayer flakes. The reversal in spontaneous photocurrent polarity is observed and associated with the out-of-plane ferroelectric polarization direction. The spontaneous photocurrent originating from the shift current is also polarization-sensitive. The amplitude of spontaneous photocurrent is further increased by one order of magnitude through vacuum annealing. Our results provide a further application potential for new-generation photodetectors based on BPVE with low power consumption and multi-dimensional optoelectronic detection.

Keywords bulk photovoltaic effect, 2D ferroelectrics, 3R α-In_2Se_3, shift current, self-powered photodetection

Citation Wang H T, Wu S Q, Chen Y, et al. Bulk photovoltaic effect in two-dimensional ferroelectric α-In_2Se_3. Sci China Inf Sci, 2025, 68(2): 122401, https://doi.org/10.1007/s11432-023-4070-8

1 Introduction

The bulk photovoltaic effect (BPVE) is a second-order nonlinear optical phenomenon observed in non-centrosymmetric materials. In contrast to the conventional photovoltaic effect, which relies on the built-in electric field of a p-n junction or Schottky junction to separate photoexcited carriers, BPVE operates without the need for a junction. This unique characteristic allows homogeneous material to generate spontaneous current under uniform illumination, enabling zero-bias operation. Furthermore, BPVE offers the potential to surpass the Shockley-Queisser limit in photoelectric conversion efficiency, as it is not constrained by the bandgap of optical absorption semiconductors [1, 2]. In addition, BPVE usually exhibits sensitivity to the polarization of incident light, making it a valuable tool for polarization detection [3–6]. Devices based on BPVE have attracted extensive attention in energy collection and photoelectric detection, because they have the advantages of simple device fabrication and high quantum efficiency [7, 8].

The BPVE was first discovered in $BaTiO_3$ crystals [3], and subsequently observed in other traditional ferroelectric materials with non-central symmetry, such as $BiFeO_3$ [9] and $LuMnO_3$ [10]. Due to their low conductivity, these materials typically exhibit low short-circuit current (I_{sc}) and high open-circuit voltage (V_{oc}). Recently, enhanced BPVE has been reported in two-dimensional (2D) materials, such as CuIn-

* Corresponding author (email: shuaiqin_wu@fudan.edu.cn, yanchen_@fudan.edu.cn, xjmeng@mail.sitp.ac.cn, wxd0130@mail.sitp.ac.cn)

P_2S_6 [11], WSe_2-BP heterostructure [12], and 3R-stacked MoS_2 [8,13]. Compared to methods involving stress regulation and van der Waals heterointerface design, the introduction of 2D ferroelectrics presents a non-destructive and controllable approach to manipulate the symmetry of 2D materials. Moreover, it was theoretically predicted that 2D ferroelectrics are natural candidates for materials that produce large shift current, which is a component of photocurrent in BPVE [14]. The shift current originates from the Berry phase differences accrued during interband transition, which is a steady dc current in non-centrosymmetric crystals even in the absence of an external electric field [15]. The 2D layered semiconductor α-In_2Se_3 is a kind of 2D ferroelectric materials, characterized by stable locked out-of-plane and in-plane polarization at room temperature [16,17]. Multilayer α-In_2Se_3 possesses a direct bandgap ($\sim$1.4 eV), ensuring strong light absorption and photoelectric response [18]. This property is advantageous for the research and application of BPVE. While α-In_2Se_3 has been extensively investigated in various applications, including photoelectric detection [19–24], optoelectronic synapses [25–27], and nonvolatile memory [28–32], direct experimental studies on the BPVE in α-In_2Se_3 remain missing. Furthermore, the majority of these studies have focused on horizontal structures, which are hardly able to meet the requirements of the high-integration optoelectronic devices.

Here, we demonstrate the BPVE in 2D ferroelectric α-In_2Se_3. The multilayer graphene/α-In_2Se_3/multilayer graphene (MLG) van der Waals heterojunction was designed and fabricated. The MLG layers were employed to modulate the polarization direction of the ferroelectric layer and to collect photocurrent generated under laser illumination. Due to the distinct alignment of energy bands associated with different out-of-plane polarization states of α-In_2Se_3, the amplitude and direction of spontaneous photocurrent vary with changes in polarization direction. It has been proven that the zero-bias photocurrent primarily arises from the shift current by changing the incident laser power density. Additionally, polarization sensitivity is confirmed at zero bias voltage, benefiting from the intrinsic properties of α-In_2Se_3 and the BPVE. These results show the application potential of 2D ferroelectric α-In_2Se_3 in the realm of low power consumption and multi-dimensional optoelectronic detection.

2 Materials and methods

Material preparation and device fabrication. Bulk single crystal graphite and α-In_2Se_3 used in the study were purchased from HQ Graphene Inc. α-In_2Se_3 and graphene flakes were mechanically exfoliated onto the polydimethylsiloxane/glass and p-doped silicon substrate covered with 285 nm silicon oxide, respectively. Then the α-In_2Se_3 flake was aligned and transferred onto the bottom graphene flake under the guidance of a microscope. The graphene flakes used as the top electrodes were patterned by electron beam lithography (EBL) and etched by oxygen plasma. The etched graphene flake was picked up by water-soluble poly(vinyl alcohol) film, and then transferred onto the α-In_2Se_3/graphene heterostructure. To prepare the device for testing, metal electrodes were defined by EBL and Cr/Au (15 nm/45 nm) were deposited by thermal evaporation. The device was annealed at 150°C for 1.5 h in the vacuum after fabrication to achieve better contacts.

Material characterization. A Lab Ram HR800 from HORIBA spectrometer and an Olympus $\times$100 objective lens was used for Raman measurements illuminated with a 514.5 nm wavelength laser. In second-harmonic generation (SHG) measurement, the mode-lock picosecond pulsed laser at the wavelength of 1064 nm was used as the fundamental pump in s-in/s-out configuration. Atomic force microscope (AFM) and piezoresponse force microscopy (PFM) measurements were performed using PFM mode by Cypher S from Asylum Research.

Electrical and optoelectronic characterization. All electrical and optoelectronic measurements were performed under ambient conditions and at room temperature. All the optoelectronic measurements were taken by an MStarter 200 optoelectronic measurement system from Maita Optoelectronic Technology Co., LTD, except for the output I-V tests that were measured by a Keithley 4200-SCS semiconductor analyzer with a Lake Shore probe station. During the polarized light response measurements, the linearly polarized incident light had a fixed angle φ with respect to the normal of the sample plane (Figure S5).

3 Results and discussion

Figure 1(a) displays two oppositely polarized atom structures of one quintuple layer (QL) α-In_2Se_3, with indium atoms and selenium atoms in yellow and blue, respectively. Each QL of 3R α-In_2Se_3 ($R3m$

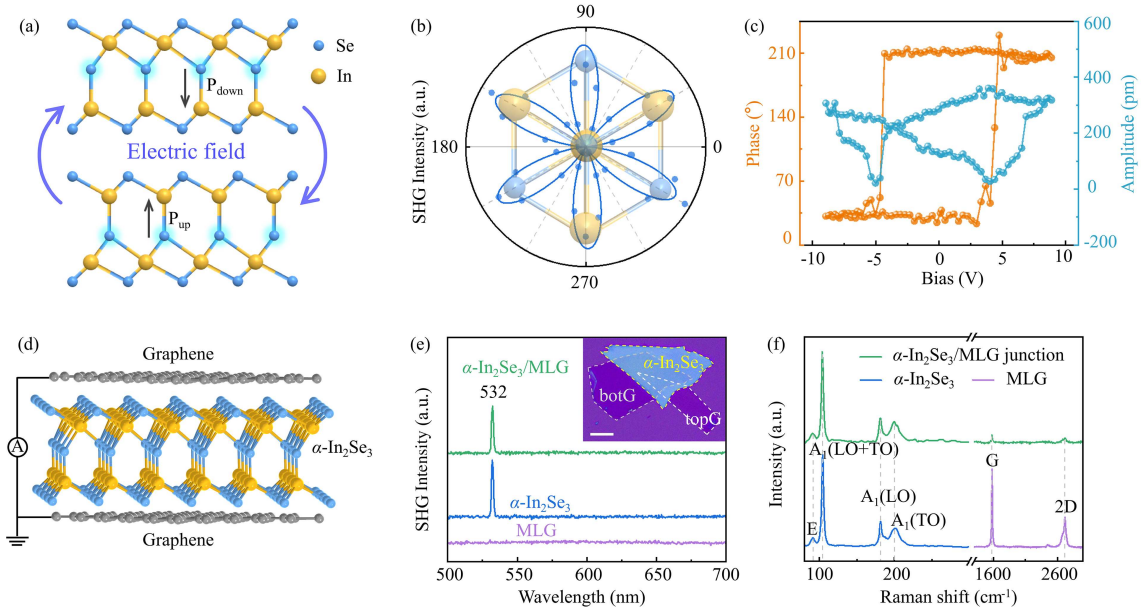

Figure 1 (Color online) Van der Waals heterostructure and ferroelectric property of α-In_2Se_3. (a) Side-view models of atom structures of one QL α-In_2Se_3 in two opposite polarizations, with indium atoms and selenium atoms in yellow and blue, respectively. The direction of spontaneous out-of-plane electric polarization is indicated by black arrows. (b) Polar plots of the polarization-resolved SHG intensity of α-In_2Se_3 in connection with the underlying crystal geometry. The blue curve is fit to $I_{2\omega} \propto \cos^2(3\theta)$. (c) Out-of-plane phase and amplitude hysteresis loop of α-In_2Se_3 using PFM. (d) Schematic illustration of the Graphene/α-In_2Se_3/Graphene heterostructure with graphene as electrodes, the photocurrent is measured through graphene electrodes. (e) The SHG spectra were collected from α-In_2Se_3, graphene, and α-In_2Se_3/Graphene heterostructure regions. Inset is the corresponding optical image of the as-stacked van der Waals heterostructure device. Top multilayer graphene (topG), bottom multilayer graphene (botG), and α-In_2Se_3 flake are indicated with dashed lines. The scale bar is 10 μm. (f) Raman spectra of α-In_2Se_3, graphene, and their heterostructure regions with 514.5 nm laser excitation. The Raman peaks corresponding to the vibration modes are marked with dashed lines.

space group) consists of five atomic layers covalently bonded in the sequence of Se-In-Se-In-Se, which is stacked in ABC type via weak van der Waals interactions. While α-In_2Se_3 in hexagonal ($P63/mmc$ space group) structure adopts an AB-type stacking order with the same QL. The asymmetric position of the intermediate Se atomic layer leads to spontaneous out-of-plane and in-plane polarization locking. The direction of out-of-plane electric polarization (indicated by black arrows in Figure 1(a)) can be reversed through an applied electric field. This process is accompanied by the breaking and formation of the In-Se covalent bonds, ensuring polarization stability [16,17]. To explore the symmetry of exfoliated 3R α-In_2Se_3 nanoflakes, polarization-resolved optical SHG measurements were performed using a picosecond pulsed laser at a wavelength of 1064 nm as the fundamental pump. The SHG intensity results, as depicted in Figure 1(b), align with the expression $I_{2\omega} \propto \cos^2(3\theta)$, where θ represents the angle between the armchair direction of α-In_2Se_3 and the polarization of the pump laser [33]. The six-fold symmetry observed in the SHG signal is indicative of C_3 rotational symmetry inherent in 3R α-In_2Se_3, consistent with its $R3m$ space group [34,35]. It is worth noting that the stronger SHG intensity along the 150° direction indicates the C_3 rotational symmetry breaking and the presence of in-plane spontaneous polarization [13]. Because of the locking between out-of-plane dipoles and in-plane lattice asymmetry in α-In_2Se_3 [17], it also means the existence of out-of-plane polarization. Besides, the maximum of each lobe coincides with the In-Se bond direction, which is also the armchair direction of the α-In_2Se_3 lattice [17]. To provide further confirmation of the ferroelectricity of 3R α-In_2Se_3, PFM measurements were conducted. The α-In_2Se_3 nanoflake with a thickness of ∼16 nm was mechanically exfoliated and transferred onto a gold substrate. As shown in Figure 1(c), the nearly 180° phase difference and the butterfly-like amplitude loop observed with varying the tip voltage clearly demonstrate the switchable ferroelectric polarization characteristic of α-In_2Se_3. It is worth noting that the coercive field is asymmetric, exhibiting a larger coercive field in the negative region, which may be associated with the downward spontaneous polarization in α-In_2Se_3. As shown in Figure S1, the coercive voltage tends to increase with the increased thickness of α-In_2Se_3. Moreover, this asymmetry could also be affected by extrinsic factors, such as the Schottky barrier difference between the upper (α-In_2Se_3/lr tip) and lower (α-In_2Se_3/Au substrate) surfaces of the sample or the presence of

adsorbates on the surface [34].

Given that the in-plane polarization of 3R α-In_2Se_3 contributes negligibly to the BPVE when the thickness exceeds three layers [36], we designed a vertical device structure of MLG/α-In_2Se_3/MLG. Two MLG layers with similar thickness were employed as transparent top and bottom electrodes to investigate switchable ferroelectric polarization and the BPVE within α-In_2Se_3 (Figure 1(d)). As shown in the inset of Figure 1(e), each mechanically exfoliated flake was stacked using an all-dry transfer technique to ensure high interface quality. To assess the impact of the transfer process on the structural integrity of 3R α-In_2Se_3, SHG and Raman spectra were performed to characterize the individual materials as well as the α-In_2Se_3/MLG junction region after the transfer operation. The SHG spectra are shown in Figure 1(e), from the region of MLG, there is no SHG signal due to its symmetrical structure. In contrast, a sharp peak at 532 nm is observed in the α-In_2Se_3/MLG or α-In_2Se_3 region, indicating that interlayer coupling between α-In_2Se_3 and MLG does not affect the symmetry and nonlinear optical properties of α-In_2Se_3 [33]. Figure 1(f) displays typical Raman peaks of α phase In_2Se_3, located at 90, 103, 181, and 201 cm^{-1}. These peaks correspond to the E symmetry mode, A_1(LO+TO), A_1(LO), and A_1(TO) phonon modes, respectively [27,34,37,38]. Notably, the presence of A_1(LO) and A_1(TO) phonon modes, resulting from LO-TO splitting, indicates that α-In_2Se_3 possesses a non-centrosymmetric structure aligning with the $R3m$ space group [37]. As for multilayer graphene, G and 2D Raman modes can be identified at about 1581 and 2717 cm^{-1}. Compared with the Raman peaks in as-exfoliated α-In_2Se_3, the same signal characteristics in the junction region demonstrate that the device fabrication process exerts no adverse effects on the lattice structure.

As a ferroelectric material, α-In_2Se_3 exhibits a spontaneous polarization orientation that can be flipped through the application of an external electric field. This polarization reversal has an impact on the energy band structure of α-In_2Se_3, subsequently influencing the motion of charge carriers. In order to explore the relationship between the polarization direction and the direction of photocurrent in the BPVE, we conducted measurements of the output current-voltage (I-V) characteristics of α-In_2Se_3 based devices under homogeneous laser irradiation at fresh, downward, and upward poled states. As depicted in Figure 2(a), under dark conditions, a linear I-V curve that intersected the origin was observed. Furthermore, when laser illumination with a wavelength of 637 nm and a power density of 5.1 W/cm^2 was applied, linear output I-V curves and evident I_{sc} or spontaneous photocurrent at zero bias were observed at different polarization states. These observations align with the typical characteristics of the output I-V curve of BPVE. Note that there are some fluctuations in the $I(V)$ data of light & P_{down} in Figure 2(a). This is because the small current level in the device may be sensitive to external factors. However, the current values are clearly distinguished, so these fluctuations do not affect the qualitative analysis of the relationship between spontaneous photocurrent and polarization of α-In_2Se_3. It is noteworthy that a zero-bias photocurrent is present in the fresh state, indicating the existence of spontaneous downward polarization in α-In_2Se_3. This observation is consistent with the SHG measurement results and accounts for the asymmetry of the PFM loop. Besides, when α-In_2Se_3 is polarized downward by applying a +2 V voltage, a negative spontaneous photocurrent is observed. Conversely, with a −2 V poling voltage, the photocurrent is modulated to a positive value. The I-V characteristics of this device during the ferroelectric polarization switching are shown in Figure S2. It can be observed that the values of the I_{sc} are different in the two oppositely polarized configurations, namely −66.7 and 23.5 pA. The decrease amplitude of spontaneous photocurrent in upward polarization can be attributed to the screening effects caused by charge transfer between the graphene and α-In_2Se_3 layers, which leads to the reduction of the electric dipoles in α-In_2Se_3 [16]. In order to increase the current level, the incident light power density and the photoresponse area can be increased. Methods such as improving the interface contact between the electrodes and the ferroelectric layer through annealing and refining the device fabrication process to increase the current level can also be considered. The V_{oc} for α-In_2Se_3 in different polarization states is −23 and 31 mV, respectively. In contrast, the V_{oc} observed in BPVE devices based on traditional ferroelectrics is larger, primarily due to their low optical conductivity [39, 40]. Because of the symmetric graphene contacts, photocurrent generated by the Schottky photovoltaic effect at the graphene/α-In_2Se_3 interface occurs in opposite directions and cancels each other out. Consequently, the dominant mechanism in our devices is not the Schottky photovoltaic effect but the BPVE, and the spontaneous photocurrent primarily arises from BPVE. Furthermore, it is worth noting that the BPVE of α-In_2Se_3 can be controllable through applying an external electric field, and the direction of the spontaneous photocurrent can change with the direction of polarization, which has also been reported in other ferroelectric materials [11,41–44].

To comprehend the underlying physical mechanism of the ferroelectric-modulated BPVE, the switch-

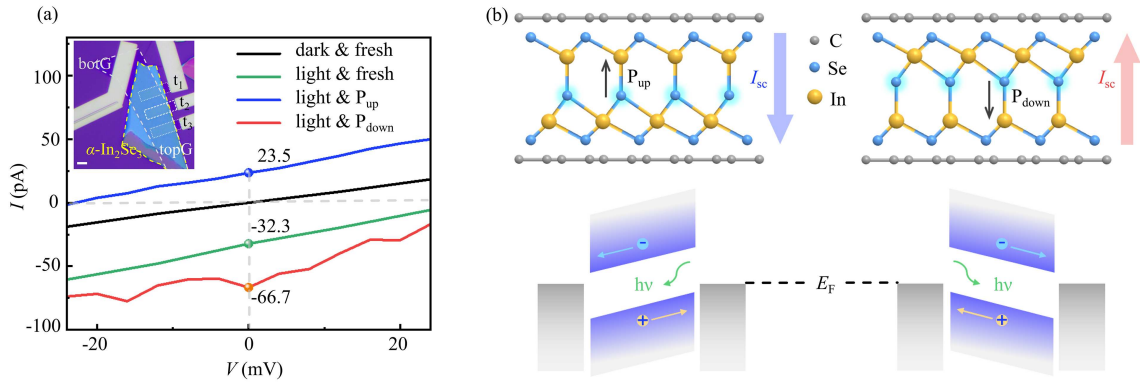

Figure 2 (Color online) Switchable photocurrent direction in α-In_2Se_3 thin layer based on BPVE. (a) The I-V characteristic curves of the MLG/α-In_2Se_3/MLG van der Waals heterostructure device at dark (black line) and bright (color lines) conditions. The blue, green, and red lines represent the upward, fresh, and downward polarized states, respectively. The inset is the optical image of an as-fabricated device with topG, botG, and α-In_2Se_3 flakes (∼35 nm) indicated with dashed lines. The top three graphene electrodes are denoted as t_1, t_2, and t_3. The scale bar is 4 μm. The poling voltage is applied to the t_2 graphene electrode and sweeps from 0 to +2 V (or −2 V) and then backward to 0 V. The reading bias is set to be within ±0.2 V. A laser with the wavelength of 637 nm is used as the excitation light source. (b) The band diagram for the MLG/α-In_2Se_3/MLG heterostructure with the ferroelectric α-In_2Se_3 at upward and downward polarization states. The top and bottom graphene electrodes are represented in gray color on the top (or left) and bottom (or right) sides of α-In_2Se_3. The direction of spontaneous out-of-plane electric polarization and short-circuit photocurrent (I_{sc}) are indicated by black arrows and color arrows, respectively. The photoexcited holes and electrons are marked with "+" and "−" symbols, respectively.

able energy band diagrams within the MLG/α-In_2Se_3/MLG heterostructure are illustrated in Figure 2(b). When the polarization of α-In_2Se_3 is poled by applying a voltage to the top MLG, the off-center displacement of Se atoms induces an out-of-plane polarization with a direction opposite to its built-in electric field (E_{bi}). The existence of out-of-plane polarization brings about variations in the vacuum levels on both sides of α-In_2Se_3, consequently leading to the tilting of its energy bands. Simultaneously, this out-of-plane polarization induces equal amounts of charge with opposite polarities in the top and bottom MLG electrodes, thus modifying the chemical potential of graphene [8]. Moreover, in the presence of graphite electrodes, the E_{bi} within the ferroelectric α-In_2Se_3 layer, induced by polarization, still maintains [16]. As a result, when the device is irradiated with light, the photo-generated electron and hole pairs are separated by E_{bi}, and drift to the interface to be collected by graphene electrodes, resulting in a significant I_{sc}. Notably, the direction of I_{sc} can be switched in accordance with the direction of electric polarization.

To further substantiate the existence of BPVE in α-In_2Se_3, we conducted a spatial distribution map of I_{sc} by scanning the device presented in Figure 3(a) under a focused 520 nm laser beam. The photo-generated current mapping image (Figure 3(b)) reveals non-zero I_{sc} exclusively within the overlapping region of the top MLG and bottom MLG electrodes, as compared with the region corresponding to the dashed box in Figure 3(a). As demonstrated in Figure 3(b), all I_{sc} values exhibit a negative polarity, signifying the downward orientation of spontaneous polarization within α-In_2Se_3. In addition, the uniform generation of I_{sc} throughout the entire overlapping area implies a uniform occurrence of the BPVE. On the contrary, at the interface between bottom MLG and α-In_2Se_3 outside the overlap region, I_{sc} is negligible, effectively excluding the contribution of Schottky photovoltaic effect to the photocurrent. Similar results have also been observed in another 2D ferroelectric material $CuInP_2S_6$ [11, 44]. For comparison, α-In_2Se_3 distinguishes itself from $CuInP_2S_6$ through its unique ferroelectric properties, including the presence of locked in-plane and out-of-plane polarization, enhanced polarization stability, and the ability to maintain a single-domain state even in ultra-thin films [45]. These characteristics, coupled with α-In_2Se_3's lower coercive field [38], higher Curie temperature [30], and broader light response spectrum due to its smaller bandgap, position α-In_2Se_3 as a superior material for low-power photodetection devices and high-temperature applications. Subsequently, we sought to investigate the origin of the photocurrent by studying its dependence on laser power density (P). A focused 520 nm laser beam with a diameter of ∼1 μm was employed to illuminate the center of the overlapping section (as shown in the inset of Figure 3(c)). Spontaneous photocurrent (I_{ph}) was obtained by averaging the photocurrent extracted from the I-t curves measured at zero bias under chopping laser irradiation. The photoresponse mechanism of the photodetector can be deduced from the power function $I_{ph} \propto P^{\alpha}$. The power dependence, visualized with a log-log plot in Figure 3(c), indicates a characteristic crossover from linear to square-root

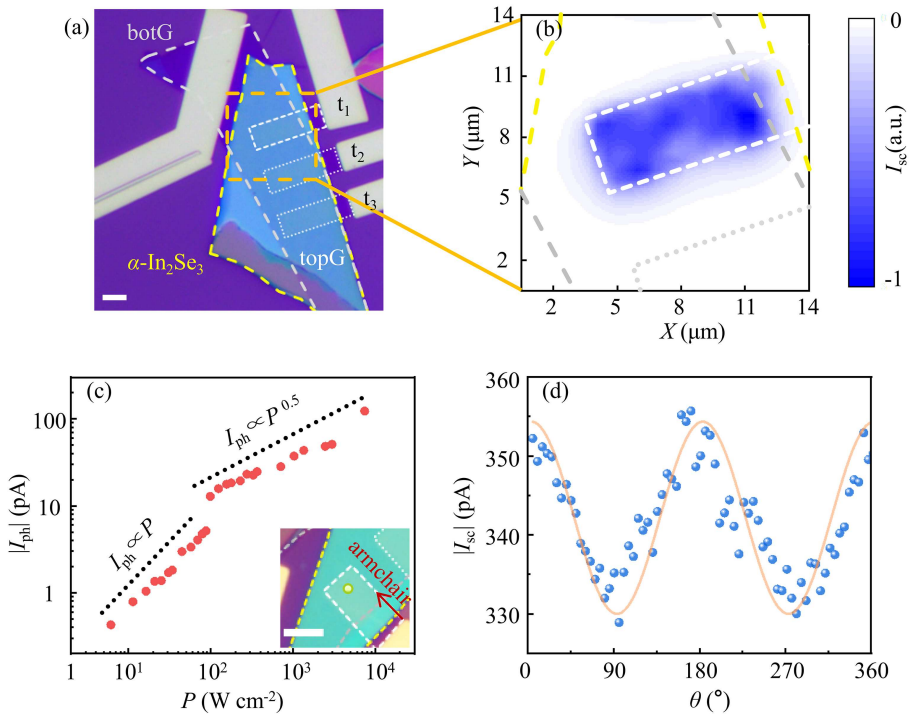

Figure 3 (Color online) Characteristics of the BPVE in α-In_2Se_3. (a) The optical image of the device. Scale bar, 4 μm. (b) Normalized short-circuit photocurrent mapping of the device corresponding to the overlapping area around the top graphene electrode t_1 and bottom graphene contact indicated with orange dashed line in (a). (c) Dependence of the spontaneous photocurrent on the incident laser power density for wavelength of 520 nm. Dashed lines serve as guidelines for linear and square-root dependence. Inset is the optical diagram of the device being tested. The green dot in the inset represents the laser spot position. Scale bar, 4 μm. (d) Laser polarization dependence of the I_{sc} of the device in the inset of (c). The excitation laser wavelength is 520 nm with the power density of 273.6 W/cm^2. Dots are experimental results and the solid line is the fitting curve fitted by the cosine function [49]. θ is the angle between light polarization and the armchair direction of α-In_2Se_3.

dependence at around 10^3 W·cm^{-2}. This feature once again suggests that the spontaneous photocurrent does not originate from the conventional Schottky photovoltaic effect but rather from the BPVE driven by the shift current mechanism [12]. The part where the amplitudes of the spontaneous photocurrent increase linearly signifies its origin from the second-order optoelectronic response to the electric field E of light ($I_{ph} \propto |E|^2 \propto P$) [46]. While the nonlinear behavior observed with increasing the intensity of monochromatic light is attributed to the effect of carrier saturation excitation, a phenomenon predicted by the shift current mechanism ($I_{ph} \propto |E| \propto P^{0.5}$) [47]. In contrast, horizontally structured devices based on α-In_2Se_3 do not exhibit such power density dependence, implying the absence of BPVE in these structures [21, 48].

On the basis of the BPVE and the anisotropic structure of α-In_2Se_3, the MLG/α-In_2Se_3/MLG device is able to achieve polarization-resolved photodetection with zero bias. In order to enhance the interface contact, the device underwent vacuum annealing prior to the polarization test. The dependence of I_{sc} on the linear polarization direction of the incident laser beam was measured, as illustrated in Figure 3(d) [49], with a wavelength of 520 nm and power density of 273.6 W/cm^2. Notably, the photocurrent of the device after annealing displayed about one-order-of-magnitude increase compared to the current before annealing under the same optical power density (Figure S4). This enhancement suggests an improved interface contact between α-In_2Se_3 and MLG [12, 48]. Considering that 2D materials usually dissociate along the zigzag direction [50], the armchair direction of α-In_2Se_3 is assigned along the red arrow (0°), as depicted in the inset of Figure 3(c). Along the direction of the red arrow, the polarization-resolved SHG reaches its maximum, which proves that this direction is the armchair direction of α-In_2Se_3 (Figure S3). The photoresponse reaches its maximum amplitude when the laser polarization aligns with the armchair (polar) direction of α-In_2Se_3, while it reaches the minimum photocurrent along the zigzag direction [24]. In addition, the cosine variation of the linear light polarization aligns well with the BPVE theoretical analysis based on the C_3 point symmetry group (see Supplementary Note). The dependence of I_{sc} on laser polarization also supports the shift current model as the origin of the photocurrent.

4 Conclusion

In conclusion, we report the observation of the BPVE in 2D ferroelectric α-In_2Se_3 and explore the origin of spontaneous photocurrent within this material. Through structural design, electrode matching, and interface treatments, the BPVE linked to the out-of-plane ferroelectricity is observed in the MLG/α-In_2Se_3/MLG van der Waals heterostructure. The direction of spontaneous photocurrent in BPVE is switchable by manipulating the polarization orientation of α-In_2Se_3 through the application of an external electric field. Besides, we demonstrate that the origin of the spontaneous photovoltaic effect is the shift current, according to the crossover of zero-bias photocurrent from a linear to square-root dependence with the increase of laser power density. Our device has also achieved zero-bias linear polarization detection, leveraging the intrinsic anisotropic structure and the BPVE of α-In_2Se_3. The amplitude of the spontaneous current has been further increased by one order of magnitude through a vacuum annealing process. Our results not only shed light on the mechanism of the BPVE in 2D ferroelectrics but also promote the future application of 2D ferroelectric materials in energy-efficient photodetection. Devices based on 2D ferroelectric semiconductors have a bright future in the realms of nonlinear optics and multi-dimensional light detection.

Supporting information Figures S1–S5 and Supplementary Note. The supporting information is available online at info.scichina.com and link.springer.com. The supporting materials are published as submitted, without typesetting or editing. The responsibility for scientific accuracy and content remains entirely with the authors.

Acknowledgements This work was supported by Strategic Priority Research Program of the Chinese Academy of Sciences (Grant No. XDB0580000), National Natural Science Foundation of China (Grant Nos. 62075228, 62025405, 62222413, 62105100, 62334001), Strategic Priority Research Program of the Chinese Academy of Sciences (Grant No. XDB44000000), China National Postdoctoral Program for Innovative Talents (Grant No. BX20230392), China Postdoctoral Science Foundation (Grant Nos. 2023M730621, 2023M743651), Shanghai Post-doctoral Excellence Program (Grant No. 2022103), Natural Science Foundation of Shanghai (Grant No. 23ZR1473400), and Hundred Talents Program of the Chinese Academy of Sciences.

References

1 Shockley W, Queisser H J. Detailed balance limit of efficiency of p-n junction solar cells. J Appl Phys, 1961, 32: 510–519
2 Spanier J E, Fridkin V M, Rappe A M, et al. Power conversion efficiency exceeding the Shockley-Queisser limit in a ferroelectric insulator. Nat Photon, 2016, 10: 611–616
3 Koch W T H, Munser R, Ruppel W, et al. Bulk photovoltaic effect in $BaTiO_3$. Solid State Commun, 1975, 17: 847–850
4 Choi T, Lee S, Choi Y J, et al. Switchable ferroelectric diode and photovoltaic effect in $BiFeO_3$. Science, 2009, 324: 63–66
5 Ma C, Yuan S, Cheung P, et al. Intelligent infrared sensing enabled by tunable Moiré quantum geometry. Nature, 2022, 604: 266–272
6 Wu S, Chen Y, Wang X, et al. Ultra-sensitive polarization-resolved black phosphorus homojunction photodetector defined by ferroelectric domains. Nat Commun, 2022, 13: 3198
7 Zhang Y J, Ideue T, Onga M, et al. Enhanced intrinsic photovoltaic effect in tungsten disulfide nanotubes. Nature, 2019, 570: 349–353
8 Yang D, Wu J, Zhou B T, et al. Spontaneous-polarization-induced photovoltaic effect in rhombohedrally stacked MoS_2. Nat Photon, 2022, 16: 469–474
9 Knoche D S, Steimecke M, Yun Y, et al. Anomalous circular bulk photovoltaic effect in $BiFeO_3$ thin films with stripe-domain pattern. Nat Commun, 2021, 12: 282
10 Sheng Y, Fina I, Gospodinov M, et al. Bulk photovoltaic effect in hexagonal $LuMnO_3$ single crystals. Phys Rev B, 2021, 104: 184116
11 Li Y, Fu J, Mao X, et al. Enhanced bulk photovoltaic effect in two-dimensional ferroelectric $CuInP_2S_6$. Nat Commun, 2021, 12: 5896
12 Akamatsu T, Ideue T, Zhou L, et al. A van der Waals interface that creates in-plane polarization and a spontaneous photovoltaic effect. Science, 2021, 372: 68–72
13 Dong Y, Yang M M, Yoshii M, et al. Giant bulk piezophotovoltaic effect in 3R-MoS_2. Nat Nanotechnol, 2023, 18: 36–41
14 Fregoso B M, Morimoto T, Moore J E. Quantitative relationship between polarization differences and the zone-averaged shift photocurrent. Phys Rev B, 2017, 96: 075421
15 Morimoto T, Nagaosa N. Topological aspects of nonlinear excitonic processes in noncentrosymmetric crystals. Phys Rev B, 2016, 94: 035117
16 Ding W, Zhu J, Wang Z, et al. Prediction of intrinsic two-dimensional ferroelectrics in In_2Se_3 and other III_2-VI_3 van der Waals materials. Nat Commun, 2017, 8: 14956
17 Xiao J, Zhu H, Wang Y, et al. Intrinsic two-dimensional ferroelectricity with dipole locking. Phys Rev Lett, 2018, 120: 227601
18 Lyu F, Sun Y, Yang Q, et al. Thickness-dependent band gap of α-In_2Se_3: from electron energy loss spectroscopy to density functional theory calculations. Nanotechnology, 2020, 31: 315711
19 Feng W, Gao F, Hu Y, et al. High-performance and flexible photodetectors based on chemical vapor deposition grown two-dimensional In_2Se_3 nanosheets. Nanotechnology, 2018, 29: 445205
20 Feng W, Gao F, Hu Y, et al. Phase-engineering-driven enhanced electronic and optoelectronic performance of multilayer In_2Se_3 Nanosheets. ACS Appl Mater Interfaces, 2018, 10: 27584–27588
21 Tang B, Hou L, Sun M, et al. UV-SWIR broad range photodetectors made from few-layer α-In_2Se_3 nanosheets. Nanoscale, 2019, 11: 12817–12828
22 Yang J, Wang F, Guo J, et al. Ultrasensitive ferroelectric semiconductor phototransistors for photon-level detection. Adv Funct Mater, 2022, 32: 2205468
23 Liu X, Wu G, Zeng J, et al. Two-dimensional α-In_2Se_3-based ferroelectric semiconductor junction for reconfigurable photodetectors. Appl Phys Lett, 2023, 122: 193101
24 Wang S, Yang Z, Wang D, et al. Strong anisotropic two-dimensional In_2Se_3 for light intensity and polarization dual-mode high-performance detection. ACS Appl Mater Interfaces, 2023, 15: 3357–3364

25 Yan T, Cai Y C, Wang Y R, et al. Near-infrared optoelectronic synapses based on a Te/α-In_2Se_3 heterojunction for neuromorphic computing. Sci China Inf Sci, 2023, 66: 160404
26 Li X, Li S, Tang B, et al. A Vi-SWIR photonic synapse with low power consumption based on WSe_2/In_2Se_3 ferroelectric heterostructure. Adv Elect Mater, 2022, 8: 2200343
27 Liu K, Zhang T, Dang B, et al. An optoelectronic synapse based on α-In_2Se_3 with controllable temporal dynamics for multimode and multiscale reservoir computing. Nat Electron, 2022, 5: 761–773
28 Wan S, Li Y, Li W, et al. Nonvolatile ferroelectric memory effect in ultrathin α-In_2Se_3. Adv Funct Mater, 2019, 29: 1808606
29 Yang H, Xiao M, Cui Y, et al. Nonvolatile memristor based on heterostructure of 2D room-temperature ferroelectric α-In_2Se_3 and WSe_2. Sci China Inf Sci, 2019, 62: 220404
30 Tang W, Zhang X, Yu H, et al. A van der Waals ferroelectric tunnel junction for ultrahigh-temperature operation memory. Small Methods, 2022, 6: 2101583
31 Jiao H, Wang X, Wu S, et al. Ferroelectric field effect transistors for electronics and optoelectronics. Appl Phys Rev, 2023, 10: 011310
32 Wang X J, Feng Z Y, Cai J W, et al. All-van der Waals stacking ferroelectric field-effect transistor based on In_2Se_3 for high-density memory. Sci China Inf Sci, 2023, 66: 182401
33 Zhang M, Han N, Zhang J, et al. Emergent second-harmonic generation in van der Waals heterostructure of bilayer MoS_2 and monolayer graphene. Sci Adv, 2023, 9: eadf4571
34 Zhou Y, Wu D, Zhu Y, et al. Out-of-plane piezoelectricity and ferroelectricity in layered α-In_2Se_3 nanoflakes. Nano Lett, 2017, 17: 5508–5513
35 Dai M, Chen H, Wang F, et al. Robust piezo-phototronic effect in multilayer γ-InSe for high-performance self-powered flexible photodetectors. ACS Nano, 2019, 13: 7291–7299
36 Tiwari R P, Birajdar B, Ghosh R K. First-principles calculation of shift current bulk photovoltaic effect in two-dimensional α-In_2Se_3. Phys Rev B, 2020, 101: 235448
37 Lewandowska R, Bacewicz R, Filipowicz J, et al. Raman scattering in α-In_2Se_3 crystals. Mater Res Bull, 2001, 36: 2577–2583
38 Wan S, Li Y, Li W, et al. Room-temperature ferroelectricity and a switchable diode effect in two-dimensional α-In_2Se_3 thin layers. Nanoscale, 2018, 10: 14885–14892
39 Ji W, Yao K, Liang Y C. Bulk photovoltaic effect at visible wavelength in epitaxial ferroelectric $BiFeO_3$ thin films. Adv Mater, 2010, 22: 1763–1766
40 Yuan H, Wang X, Lian B, et al. Generation and electric control of spin-valley-coupled circular photogalvanic current in WSe_2. Nat Nanotech, 2014, 9: 851–857
41 Nakamura M, Horiuchi S, Kagawa F, et al. Shift current photovoltaic effect in a ferroelectric charge-transfer complex. Nat Commun, 2017, 8: 281
42 Ogawa N, Sotome M, Kaneko Y, et al. Shift current in the ferroelectric semiconductor SbSI. Phys Rev B, 2017, 96: 241203
43 Huang P J, Taniguchi K, Miyasaka H. Bulk photovoltaic effect in a pair of chiral-polar layered perovskite-type lead iodides altered by chirality of organic cations. J Am Chem Soc, 2019, 141: 14520–14523
44 Zhang Y, Taniguchi R, Masubuchi S, et al. Switchable out-of-plane shift current in ferroelectric two-dimensional material $CuInP_2S_6$. Appl Phys Lett, 2022, 120: 013103
45 Cui C, Hu W J, Yan X, et al. Intercorrelated in-plane and out-of-plane ferroelectricity in ultrathin two-dimensional layered semiconductor In_2Se_3. Nano Lett, 2018, 18: 1253–1258
46 Duan S, Qin F, Chen P, et al. Berry curvature dipole generation and helicity-to-spin conversion at symmetry-mismatched heterointerfaces. Nat Nanotechnol, 2023, 18: 867–874
47 Morimoto T, Nagaosa N. Topological nature of nonlinear optical effects in solids. Sci Adv, 2016, 2: e1501524
48 Lyu F, Li X, Tian J, et al. Temperature-driven α-β phase transformation and enhanced electronic property of 2H α-In_2Se_3. ACS Appl Mater Interfaces, 2022, 14: 23637–23644
49 Jiao H, Wang X, Chen Y, et al. HgCdTe/black phosphorus van der Waals heterojunction for high-performance polarization-sensitive midwave infrared photodetector. Sci Adv, 2022, 8: eabn1811
50 Guo Y, Liu C, Yin Q, et al. Distinctive in-plane cleavage behaviors of two-dimensional layered materials. ACS Nano, 2016, 10: 8980–8988